

Electronic Supplementary Information

Ultrawhite structural starch film for sustainable cooling

Yang Liu ^a, Andrew Caratenuto ^a, Xuguang Zhang ^a, Ying Mu ^a, Youssef Jeyar ^{b,c},

Mauro Antezza ^{b,c} and Yi Zheng ^{a,d*}

*^aDepartment of Mechanical and Industrial Engineering, Northeastern University,
Boston, MA 02115, USA*

*^bLaboratoire Charles Coulomb (L2C), UMR 5221 CNRS-Université de Montpellier, F-
34095 Montpellier, France*

^cInstitut Universitaire de France, 1 rue Descartes, F-75231, Paris Cedex 05, France

*^dDepartment of Chemical Engineering, Northeastern University, Boston, MA 02115,
USA*

*Electronic mail: y.zheng@northeastern.edu

S1 Material and methods

Fabrication of cooling starch film

Judee's Unmodified Potato Starch 2.5 lb was obtained from Amazon. The starch sample was prepared as follows: 8 g potato starch was dissolved in 100 g deionized water at 150 °C under mechanical stirring 50 min to form the homogeneous and transparent starch paste solution. The obtained solution was poured into a ring-shaped metal mold with a diameter of 70 mm and a thickness of about 10 mm. Then, the metal mold with starch paste solution was placed on top of a cold metal cylinder which was pre-cooled by the surrounding liquid N₂. After freeze-drying for 60 h in the freeze drier (Labconco-195) at a temperature of -105 °C and a pressure of 0.5 Pa, the cooling starch sample was obtained. Then, the freeze-dried samples were pressed into thin films using a hydraulic press machine (DABPRESS, 10 tons) at varying pressures.

Material characterizations

The directional-hemispherical spectral reflectance $R(\lambda)$ and transmittance $T(\lambda)$ of cooling starch films were measured in two wavelength ranges. The range of 0.3–2.5 μm was measured using a spectrometer (Jasco V770), while the mid-infrared wavelength ranges of 2.5–18 μm were obtained using the FTIR spectrometer (Jasco 6600). Additionally, the surface morphologies of cooling starch films were characterized using a scanning electron microscope (SEM, Supra 25).

Outdoor cooling temperature measurements

All experimental samples were placed individually on polystyrene plates measuring 20 cm \times 20 cm \times 5 cm, which have good thermal insulation performance (thermal conductivity of 0.027 W/m/K). The insulation was covered with aluminum foil to

reflect sunlight from the insulation and avoid excess heating. No additional wind covering was used to minimize non-radiative heat transfer (e.g. conduction and convection) from the surrounding air. To prevent heat conduction from the ground, all testing boxes were positioned on a trolley elevated to a height of 1.5 meters and covered with aluminum foil. K-type thermocouples were affixed to the backside of each sample at their respective center points to accurately measure the sample temperatures.

Mechanical strength measurement

The mechanical strength of the cooling starch film (20 mm × 1.5 mm × 0.8 mm) and a balsa wood sheet (20 cm × 1.5 mm × 0.8 mm) were measured using a Ta Instruments DMA RSA G2 at room temperature.

Calculation of solar absorptance and thermal emittance

The average solar reflectance \bar{R}_{solar} is a function of wavelength and incidence angle, and is defined as:¹

$$\bar{R}_{\text{solar}}(\lambda, \theta) = \frac{\int_{0.3\mu\text{m}}^{2.5\mu\text{m}} I_{\text{solar}}(\lambda) \cdot R(\lambda, \theta) d\lambda}{\int_{0.3\mu\text{m}}^{2.5\mu\text{m}} I_{\text{solar}}(\lambda) d\lambda} \quad (1)$$

where λ is the wavelength of incident solar radiation over the range of 0.3–2.5 μm and $R(\lambda, \theta)$ is the surface's spectral directional reflectance.

The average thermal emittance $\bar{\epsilon}_{IR}$ within atmospheric transparency window ($\lambda \sim 8\text{--}13 \mu\text{m}$) is defined as:¹

$$\bar{\varepsilon}_{IR}(\lambda, \theta) = \frac{\int_{8\mu m}^{13\mu m} I_{BB}(\lambda) \cdot \varepsilon_{LWIR}(\lambda, \theta) d\lambda}{\int_{8\mu m}^{13\mu m} I_{BB}(\lambda) d\lambda} \quad (2)$$

where $I_{BB}(\lambda)$ is the spectral radiation intensity of a blackbody, and $\varepsilon_{IR}(\lambda, \theta)$ is the surface's spectral directional thermal emittance from 8–13 μm .

S2 Theoretical calculation of the radiative cooling power

When a cooling starch film is directly exposed to sunlight, the net cooling power P_{cool} of the cooling starch film can be described as:^{2,3}

$$P_{cool}(T_{cooler}) = P_{rad}(T_{cooler}) - P_{atm}(T_{amb}) - P_{solar} - P_{nr}, \quad (3)$$

where T_{cooler} and T_{amb} are the cooling starch film temperature and the ambient temperature, respectively. $P_{rad}(T_{cooler})$ is the radiative cooling power emitted by the cooling starch film, and $P_{atm}(T_{amb})$ is the incident radiative power from the ambient absorbed by the cooling starch film. P_{solar} and P_{nr} are the solar power absorbed by the cooling starch film and the non-radiative power from the ambient heat convection and conduction, respectively. Here, $P_{rad}(T_{cooler})$, $P_{atm}(T_{amb})$, P_{solar} and P_{nr} can be described as below:

$$P_{rad}(T_{cooler}) = A \int d\Omega \cos^2 \theta \int_0^{\infty} d\lambda I_{BB}(T_{cooler}, \lambda) \varepsilon(\lambda, \theta) \quad (4)$$

$$P_{atm}(T_{amb}) = A \int d\Omega \cos^2 \theta \int_0^{\infty} d\lambda I_{BB}(T_{amb}, \lambda) \varepsilon(\lambda, \theta) \varepsilon_{atm}(\lambda, \theta) \quad (5)$$

$$P_{solar} = A \int_0^{\infty} d\lambda \varepsilon(\lambda, \theta_{solar}) I_{AM1.5}(\lambda) \quad (6)$$

$$P_{nr}(T_{cooler}, T_{amb}) = Ah_{nr}(T_{amb} - T_{cooler}), \quad (7)$$

where $I_{BB}(T_{cooler}, \lambda) = \frac{2hc^2}{\lambda^5} \frac{1}{e^{hc/(\lambda k_B T)} - 1}$ is the spectral blackbody radiation from

Planck's Law. $\varepsilon(\lambda, \theta)$ and $\varepsilon_{\text{atm}}(\lambda, \theta) = 1 - t(\lambda)^{1/\cos \theta}$ are the directional emissivities of the cooling starch surface and atmosphere, respectively. In Eq. (6), $I_{\text{AM1.5}}(\lambda)$ is the spectral incident solar irradiance at AM 1.5. In Eq. (7), the non-radiative heat coefficient $h_{nr} = h_{\text{cond}} + h_{\text{conv}}$ considers the heat conduction and convection from the ambient (0–10 W/m²/K).^{4,5}

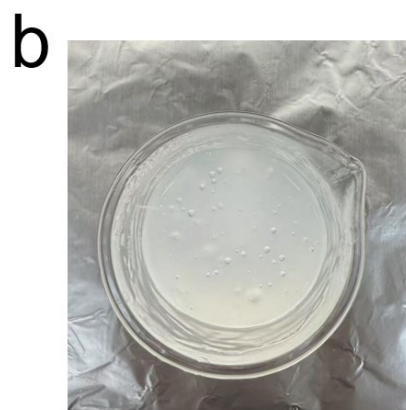


Fig. S1 (a) Experimental setup for heating the starch solution, and (b) appearance of the starch solution after gelatinization.

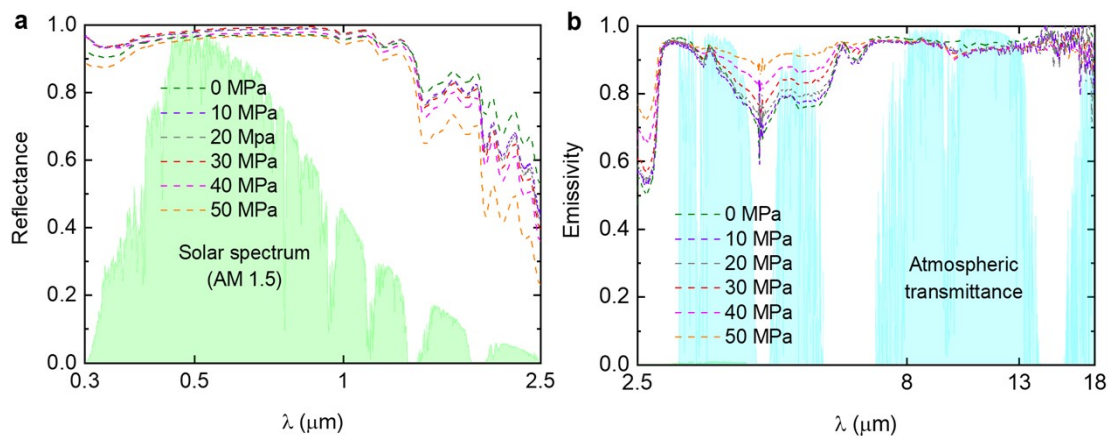


Fig. S2 Optical properties of six cooling starch films under different mechanical pressures. (a) Solar reflectance and (b) infrared thermal emissivity of Starch_{0MPa}, Starch_{10MPa}, Starch_{20MPa}, Starch_{30MPa}, Starch_{40MPa} and Starch_{50MPa} within the atmospheric transparency window.

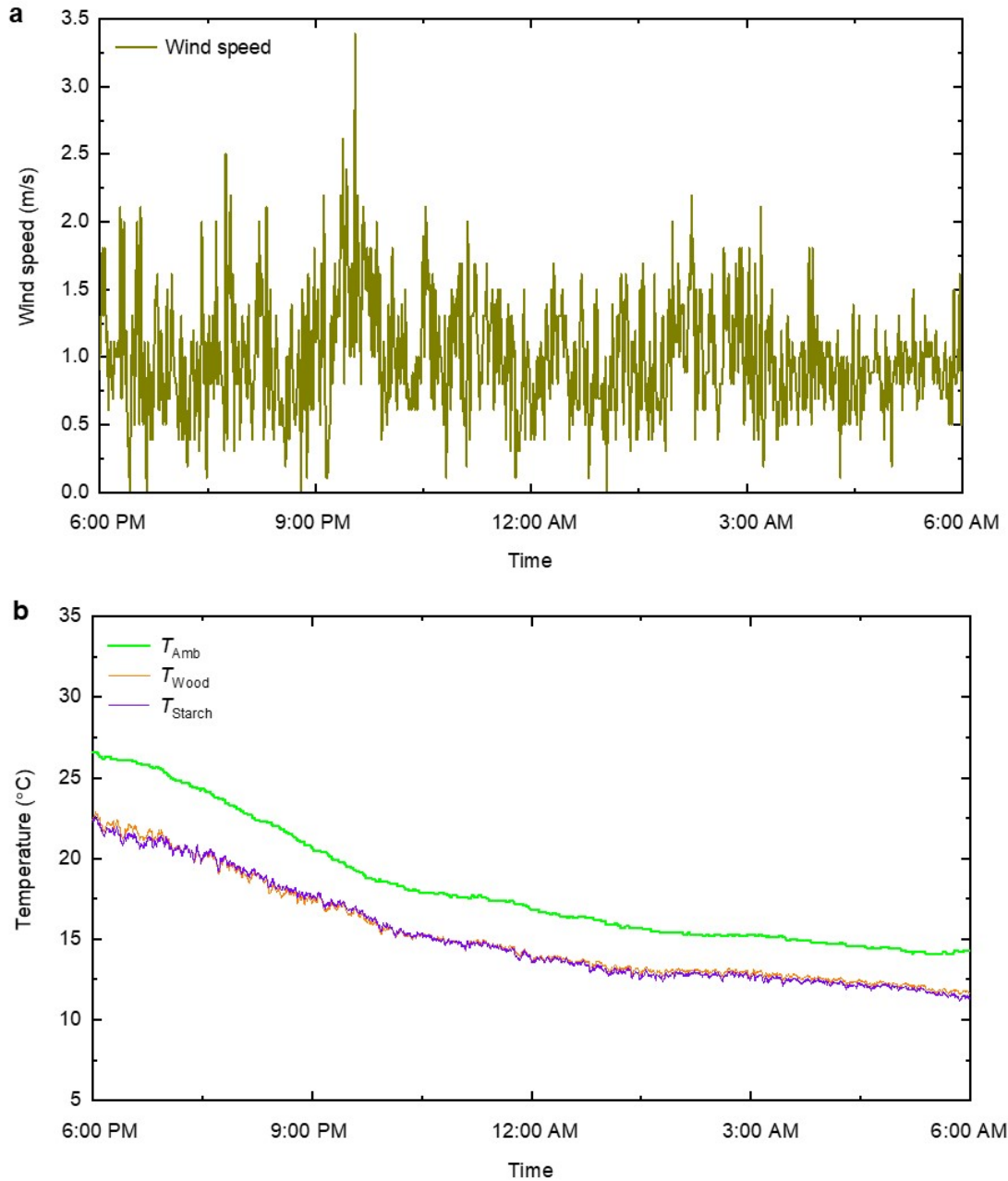


Fig. S3 Outdoor radiative cooling experiment of the cooling starch film at nighttime, in Boston, USA (42.36° N, 71.06° W) from May 31 to June 1, 2023. (a) Real-time wind speed and (b) temperatures for the ambient air, wood sheet, and cooling starch film during the experimental period.

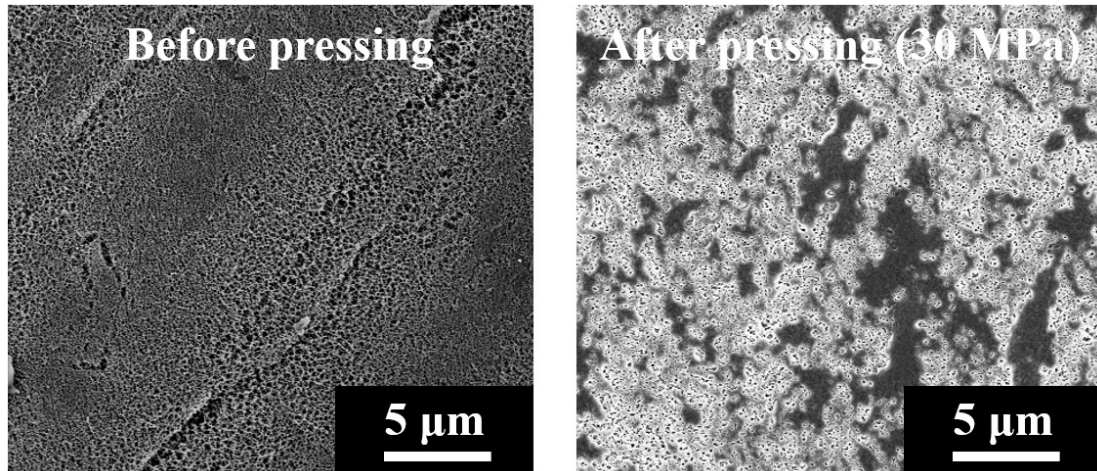


Fig. S4 Surface characterizations of cooling starch film. SEM images of starch film before and after pressing.

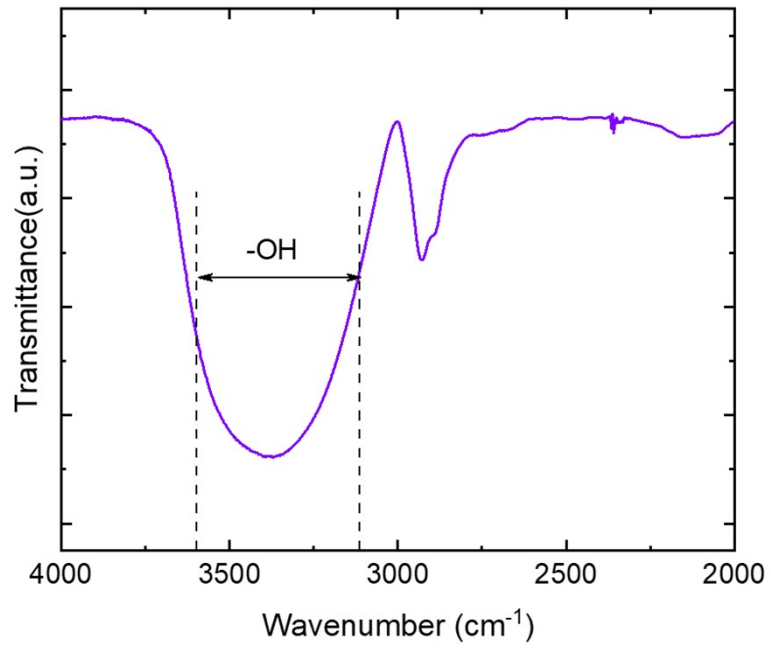


Fig. S5 FTIR transmittance spectrum of the cooing starch film presenting -OH stretching.

Table S1 Comparison of density and porosity for Starch_{0MPa}, Starch_{30MPa}, Starch_{40MPa}, and Starch_{50MPa}.

	Starch _{0MPa}	Starch _{30MPa}	Starch _{40MPa}	Starch _{50MPa}
Density (g/cm ³)	0.11	1.10	1.16	1.25
Porosity (%)	92.83	28.35	22.86	16.69

Table S2 Comparison of PDRC performances of the radiative coolers.

Materials	Structure	Solar reflectance/thermal emittance	Solar intensity (W/m ²)	Relative humidity (%)	Temperature drop (°C)	Cooling power (W/m ²)	Year
P(Vdf-HFP) ⁶	hierarchical pore	0.96/0.97	890	dry	6	96	2018
Wood ⁷	porous structure	0.96/-	<750	-	4	16	2019
PMM ⁸	micropore array/random nanopores	0.95/0.98	860 930	38 64	8.9 5.5	85	2020
PDMS ⁹	porous structure	-/0.96	<1000	-	4.6	43	2021
PTFE/cellulose paper ¹⁰	porous structure	0.99/>0.90	834	55.3	5	104	2021
PMMA ¹¹	OPA structure	0.85/0.98	850	40	8.1	-	2022
Hydroxyapatite Fiber ¹²	porous structure	0.99/0.90	860	30	5.1	104	2022
Glass/Al ₂ O ₃ ¹³	porous structure	0.96/0.95	790	30	3.5	60	2023
Ceramic ¹⁴	porous structure	0.996/0.965	800	50	>4°C	>130	2023
PMMA ¹⁵	gradient porous structure	0.99/0.97	780	40	8.2	90	2024
This work	porous structure	0.96/0.94	643	45	6.8	87	2025

S3 Stability of the cooling starch film for outdoor application

We acknowledge that the pure-natural radiative cooling starch film presented in this work lacks waterproofing capability, which limits its direct applicability in outdoor environments, particularly in rainy conditions. As shown in Fig. S6, the cooling starch film dissolved in water during the immersion test.

To begin with, we recognized that natural potato starch is not inherently waterproof, making it challenging to use on its own for outdoor applications without additional treatment. However, our objective was not to address waterproofing but rather to demonstrate that starch—a widely available biomaterial—can be processed into an optical material with exceptional radiative cooling capacity. By utilizing a porous structure formed through gelatinization, freeze-drying, and densification, we showcased the potential of natural starch as a sustainable radiative cooling material. Therefore, this work represents a foundational step in adapting starch-based materials for eco-friendly radiative cooling materials.

Several well-established methods can improve the waterproofing of cooling starch film, such as encapsulation with transparent commercial films (e.g., polyethylene thin films)¹⁶, polymeric coatings (e.g., air-spraying plastic microparticles atop the materials)¹⁰, and chemical surface treatment (e.g., fluorosilane treatment)⁷. Here, we wrapped the starch film with a commercial PE film to enhance its waterproofing. Fig. S7 presents the spectral reflectance of the cooling starch film with and without a commercial PE film covering. While the commercial PE film slightly reduces infrared emission, it does not significantly affect the solar reflectance of the cooling starch film. Thus, this method effectively addresses the waterproofing challenge for the outdoor application of cooling starch film.

Additionally, we presented an additional method to enhance the waterproofing of the

cooling starch film by air-spraying ethanolic poly(tetrafluoroethylene) (PTFE) microparticle (1.4 μm average size in diameter, Sigma-Aldrich) suspensions on the cooling starch film. The PTFE coating can significantly improve the hydrophobicity of the cooling starch film. For detailed experimental methods, please refer to the literature¹⁰. Although the PTFE coating slightly reduces the solar reflectance of cooling starch film, it forms a rough surface with micro/nanostructures, transforming the cooling starch film from a hydrophilic to a highly hydrophobic ($\theta = 147^\circ$) (Fig. S8 and Video S1). This feature enables the cooling starch film to have a waterproof surface, making it suitable for outdoor applications. Therefore, these methods potentially address the waterproofing challenge for the outdoor application of the cooling starch film.

While these strategies can enhance the durability of the cooling starch film, they often involve costly or environmentally harmful synthetic chemicals and plastic components, which contradict the core motivation of this work. Our primary objective is to highlight the intrinsic optical properties and radiative cooling capacity of pure-natural starch film. Therefore, we deliberately avoided introducing additional materials to improve outdoor durability in this study. This work serves as an initial step in transforming a single natural material into a radiative cooling material, opening new possibilities for sustainable cooling solutions.

Additionally, to test the long-term durability of the cooling starch film under sunlight, the cooling starch film was placed in a UV lamp (SVCUV 365 nm 15 W) for 50 hours, as shown in Fig. S9. It is obvious that after 50-hour UV exposure, only a slight change in the solar reflectance was observed. This result demonstrates that the cooling starch film exhibits good stability under sunlight, helping to preserve its cooling performance in real-world applications.

The core objective of this work was to demonstrate the feasibility of utilizing a single natural starch to develop an optical material with high solar reflectance and strong

infrared emission. By highlighting the potential of starch in the field of radiative cooling, we hope to inspire future research aimed at optimizing its properties for practical outdoor applications. Future studies could explore strategies to enhance its durability while maintaining its biodegradable and environmentally friendly nature. We believe this work lays the groundwork for further advancements in natural-material-based cooling technologies and encourages the scientific community to explore sustainable pathways for next-generation sustainable passive cooling materials.

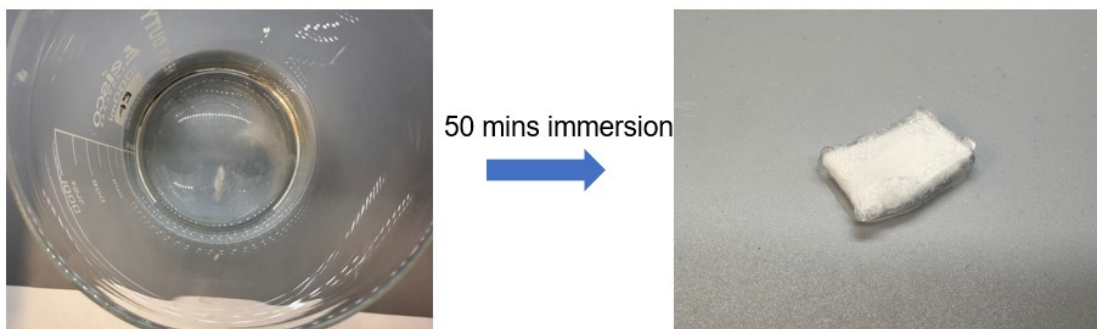


Fig. S6 Water immersion test. Cooling Starch film is immersed in DI water in a beaker.

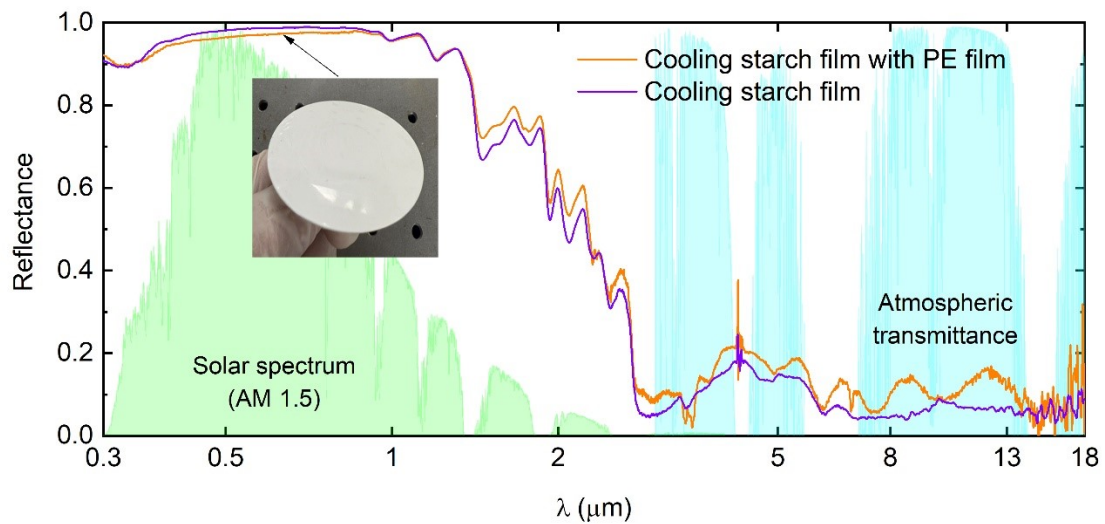


Fig. S7 Spectral reflectance of the cooling starch film with and without a commercial PE film covering.

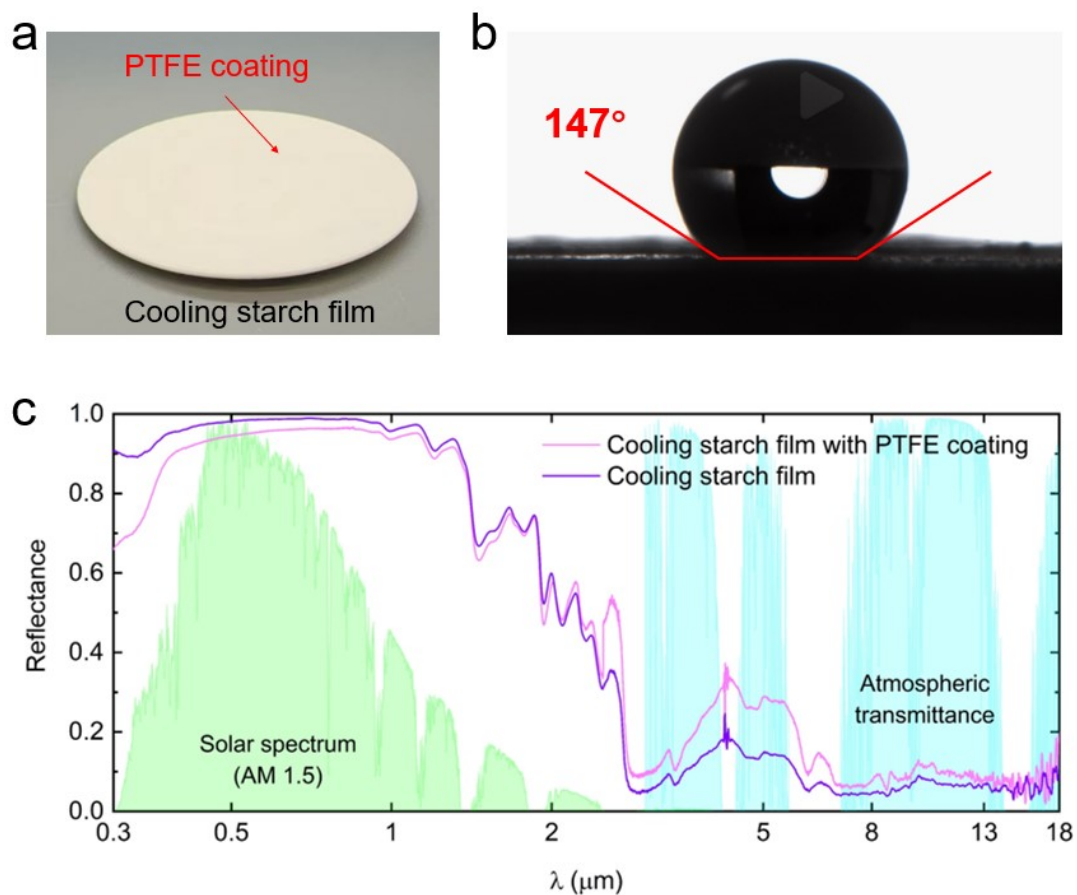


Fig. S8 (a) Optical image and (b) water contact angle image of the PTFE-coated cooling starch film. (c) Spectral reflectance of the cooling starch film with and without PTFE coating.

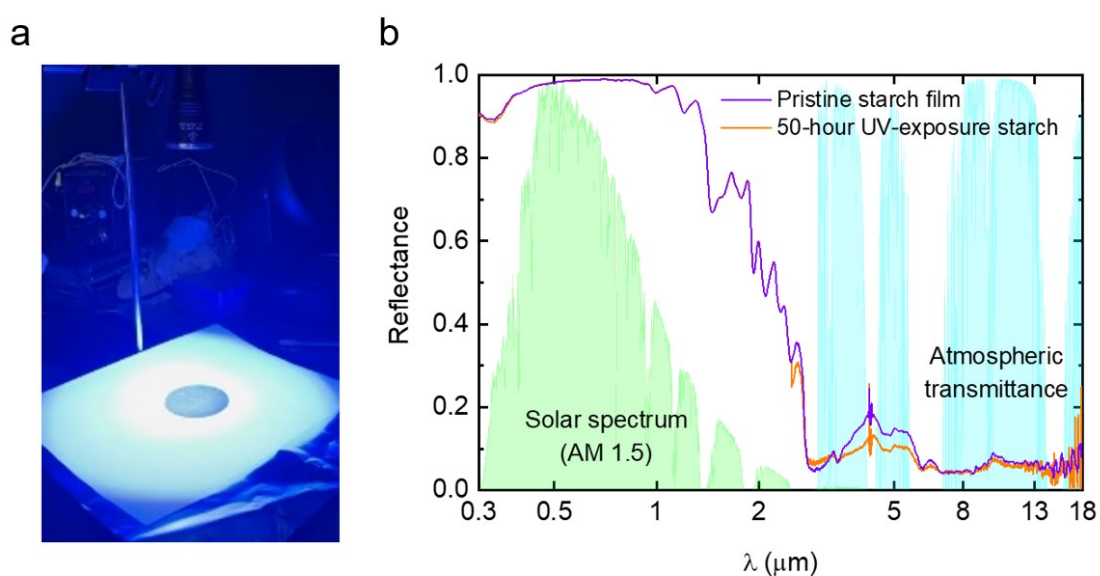


Fig. S9 UV exposure of the starch cooling film. (a) Setup of the UV exposure. (b)

Reflectivity spectra of the starch cooling film before and after 50-hour UV exposure.

Reference

- 1 H. Zhao, Q. Sun, J. Zhou, X. Deng, J. Cui, *Adv. Mater.* 2020, **32**, 2000870.
- 2 B. Zhao, M. Hu, X. Ao, N. Chen, G. Pei, *Appl. Energy* 2019, **236**, 489-513.
- 3 S. Fan, W. Li, *Nat. Photon.* 2022, **16**, 182-190.
- 4 T. Wang, Y. Wu, L. Shi, X. Hu, M. Chen, L. Wu, *Nat. Commun.* 2021, **12**, 365.
- 5 X. Liu, Y. Tian, F. Chen, A. Ghanekar, M. Antezza, Y. Zheng, *Communications Materials* 2020, **1**, 95.
- 6 J. Mandal, Y. Fu, A. C. Overvig, M. Jia, K. Sun, N. N. Shi, H. Zhou, X. Xiao, N. Yu, Y. Yang, *Science* 2018, **362**, 315-319.
- 7 T. Li, Y. Zhai, S. He, W. Gan, Z. Wei, M. Heidarinejad, D. Dalgo, R. Mi, X. Zhao, J. Song, *Science* 2019, **364**, 760-763.
- 8 T. Wang, Y. Wu, L. Shi, X. Hu, M. Chen, L. Wu, *Nat. Commun.* 2021, **12**, 1-11.
- 9 L. Zhou, J. Rada, H. Zhang, H. Song, S. Mirniaharikandi, B. S. Ooi, Q. Gan, *Adv. Sci.* 2021, **8**, 2102502.
- 10 Y. Tian, H. Shao, X. Liu, F. Chen, Y. Li, C. Tang, Y. Zheng, *ACS Appl. Mater. Interfaces* 2021, **13**, 22521-22530.
- 11 G. Qi, X. Tan, Y. Tu, X. Yang, Y. Qiao, Y. Wang, J. Geng, S. Yao, X. Chen, *ACS Appl. Mater. Interfaces* 2022, **14**, 31277-31284.
- 12 Y. Tian, X. Liu, Z. Wang, J. Li, Y. Mu, S. Zhou, F. Chen, M. L. Minus, G. Xiao, Y. Zheng, *Nano Energy* 2022, **96**, 107085.
- 13 X. Zhao, T. Li, H. Xie, H. Liu, L. Wang, Y. Qu, S. C. Li, S. Liu, A. H. Brozena, Z. Yu, *Science* 2023, **382**, 684-691.
- 14 K. Lin, S. Chen, Y. Zeng, T. C. Ho, Y. Zhu, X. Wang, F. Liu, B. Huang, C. Y.-H. Chao, Z. Wang, *Science* 2023, **382**, 691-697.
- 15 Y. Liu, A. Caratenuto, F. Chen, Y. Zheng, *Chem. Eng. J.* 2024, 150657.
- 16 Y. Tian, X. Liu, F. Chen, Y. Zheng, *Sol. Energy Mater. Sol. Cells* 2021, **230**, 111286.